

---

# Gradient descent induces alignment between weights and the empirical NTK for deep non-linear networks

---

Daniel Beaglehole<sup>†1</sup> Ioannis Mitliagkas<sup>2,3</sup> Atish Agarwala<sup>2</sup>

## Abstract

Understanding the mechanisms through which neural networks extract statistics from input-label pairs is one of the most important unsolved problems in supervised learning. Prior works have identified that the gram matrices of the weights in trained neural networks of general architectures are proportional to the average gradient outer product of the model, in a statement known as the *Neural Feature Ansatz* (NFA). However, the reason these quantities become correlated during training is poorly understood. In this work, we explain the emergence of this correlation. We identify that the NFA is equivalent to alignment between the left singular structure of the weight matrices and a significant component of the empirical neural tangent kernels associated with those weights. We establish that the NFA introduced in prior works is driven by a centered NFA that isolates this alignment. We show that the speed of NFA development can be predicted analytically at early training times in terms of simple statistics of the inputs and labels. Finally, we introduce a simple intervention to increase NFA correlation at any given layer, which dramatically improves the quality of features learned.

## 1. Introduction

Neural networks have emerged as the state-of-the-art machine learning methods for seemingly complex tasks, such as language generation (Brown et al., 2020), image classification (Krizhevsky et al., 2012), and visual rendering (Mildenhall et al., 2021). The precise reasons why neural networks generalize well have been the subject of intensive exploration, beginning with the observation that standard generalization bounds from statistical learning theory fall

short of explaining their performance (Zhang et al., 2021).

A promising line of work emerged in the form of the *neural tangent kernel* (NTK), connecting neural networks to kernels in the wide limit (Jacot et al., 2018; Chizat et al., 2019). However, subsequent research showed that the success of neural networks relies critically on aspects of learning which are absent in kernel approximations (Ghorbani et al., 2019; Allen-Zhu and Li, 2019; Yehudai and Shamir, 2019; Li et al., 2020; Refinetti et al., 2021). Other work showed that low width suffices for gradient descent to achieve arbitrarily small test error (Ji and Zhu, 2020), further refuting the idea that extremely wide networks are necessary.

Subsequently, the success of neural networks has been largely attributed to *feature learning* - the ability of neural networks to learn statistics, measurements, and representations of data which are useful for downstream tasks. However, the specific mechanism through which features are learned is an important unsolved problem in deep learning theory. A number of works have studied the abilities of neural networks to learn features in structured settings (Abbe et al., 2022; Ba et al., 2022; Nichani et al., 2023; Barak et al., 2022; Damian et al., 2022; Moniri et al., 2023; Parkinson et al., 2023). Some of that work proves strict separation in terms of sample complexity between neural networks trained with stochastic gradient descent and kernels (Mousavi-Hosseini et al., 2022).

The work above studies simple structure, such as learning from low-rank data or functions that are hierarchical compositions of simple elements. Recent work makes a big step towards generalizing these assumptions by proposing the *neural feature ansatz* (NFA) (Radhakrishnan et al., 2022; Beaglehole et al., 2023), a general structure that emerges in the weights of trained neural networks. The NFA states that the gram matrix of the weights at a given layer (known as the *neural feature matrix* (NFM)) is aligned with the *average gradient outer product* (AGOP) of the network with respect to the input to that layer. In particular, the NFM and AGOP are highly correlated in all layers of trained neural networks of general architectures, including practical models such as AlexNet (Krizhevsky et al., 2012) and VGG (Simonyan and Zisserman, 2014).

---

<sup>†</sup>Work done while interning at Google DeepMind <sup>1</sup>Computer Science and Engineering, UC San Diego <sup>2</sup>Google DeepMind <sup>3</sup>Mila, Université de Montréal. Correspondence to: Daniel Beaglehole <dbeaglehole@ucsd.edu>.

A major missing element of this theory is the reason the AGOP and NFM become correlated during training. In this paper, we explain the emergence of this correlation. We establish that the NFA is equivalent to alignment between the left singular structure of the weight matrices and the *pre-activation neural tangent kernel* (PTK), which is closely related to *empirical neural tangent kernel* (ENTK) (Section 2). By introducing a modified NFA, we demonstrate that the original NFA is driven by alignment of the left singular vectors of the weight matrices to with the PTK (Section 2). Further, we show that the alignment speed can be understood analytically in terms of the statistics of the data and labels at early times, and can be manipulated theoretically (Section 3).

Finally, we force the strength of the NFA alignment to improve using two interventions: small initialization and Speed Limited Optimization, a layerwise gradient normalization scheme (Section 4). This suggests a path towards rational design of architectures and training procedures that maximize this notion of feature learning.

## 2. Alignment between the weight matrices and the empirical NTK

### 2.1. Preliminaries

We consider fully-connected neural networks with a single output of depth  $L \geq 1$ , where  $L$  is the number of hidden layers, written  $f : \mathbb{R}^d \rightarrow \mathbb{R}$ . We write the input to layer  $\ell \in \{0, \dots, L-1\}$  as  $x_\ell$ , where  $x_0 \equiv x$  is the original datapoint, and the pre-activation as  $h_\ell(x)$ . Then,

$$h_\ell(x) = W^{(\ell)} x_\ell, \quad x_{\ell+1} = \phi(h_\ell(x)),$$

where  $\phi$  is an element-wise nonlinearity,  $W^{(\ell)} \in \mathbb{R}^{k_{\ell+1} \times k_\ell}$  is a weight matrix, and  $k_\ell$  is the hidden dimension at layer  $\ell$ . We restrict  $k_{L+1}$  to be the number of output logits, and set  $k_0 = d$ , where  $d$  is the input dimension of the data. Note that  $f(x) = h_{L+1}(x)$ . We train  $f$  by gradient descent on a loss function  $\mathcal{L}(\theta, X)$ , where  $X$  is an input dataset, and  $\theta$  is the collection of weights.

We consider a supervised learning setup where we are provided  $n$  input-label pairs  $(x^{(1)}, y^{(1)}), \dots, (x^{(n)}, y^{(n)}) \in \mathbb{R}^d \times \mathbb{R}$ . We denote the inputs  $X \in \mathbb{R}^{n \times d}$  and the labels  $y \in \mathbb{R}^{n \times 1}$ . We train a fully-connected neural network to learn the mapping from inputs to labels by minimizing a standard loss function, such as mean-squared-error or cross-entropy, on the dataset.

One can define two objects associated with neural networks that capture learned structure. For a given layer  $\ell$ , the *neural feature matrix* (NFM)  $F_\ell$  is the gram matrix of the columns of the weight matrix  $W^{(\ell)}$ , i.e.  $F_\ell \equiv (W^{(\ell)})^\top W^{(\ell)}$ . The second fundamental object we consider is the *average gradient outer product* (AGOP)  $\bar{G}_\ell$ , defined

as  $\bar{G}_\ell \equiv \frac{1}{n} \sum_{\alpha=1}^n \frac{\partial f(x_\ell^{(\alpha)})}{\partial x_\ell} \frac{\partial f(x_\ell^{(\alpha)})^\top}{\partial x_\ell}$ . To understand the structure of these objects, consider the following *chain-monomial* low-rank task:

$$y(x) = \sum_{k=1}^r x_{k \bmod r} \cdot x_{(k+1) \bmod r}, \quad (1)$$

where the data inputs are sampled from an isotropic Gaussian distribution  $\mu = \mathcal{N}(0, I)$ . In this case, both objects capture the coordinates on which the target function depends (Figure 1). Prior work has shown that in trained neural networks, these objects will be proportional to each other to varying degree of approximation. This notion is formalized in the *Neural Feature Ansatz* (NFA):

**Ansatz 1** (Neural Feature Ansatz (Radhakrishnan et al., 2022)). *The Neural Feature Ansatz states that, for all layers  $\ell \in [L]$  of a fully-connected neural network with  $L$  hidden layers trained on input data  $x^{(1)}, \dots, x^{(n)}$ ,*

$$(W^{(\ell)})^\top W^{(\ell)} \propto \frac{1}{n} \sum_{\alpha=1}^n \frac{\partial f(x_\ell^{(\alpha)})}{\partial x_\ell} \frac{\partial f(x_\ell^{(\alpha)})^\top}{\partial x_\ell},$$

The left and right hand sides of this equation are the NFM and AGOP with respect to the input of layer  $\ell$ . Here,  $\frac{\partial f(x)}{\partial x_\ell} \in \mathbb{R}^{k_\ell \times 1}$  denotes the gradient of the function  $f$  with respect to the intermediate representation  $x_\ell$ . For simplicity, we may concatenate these gradients into a single matrix  $\frac{\partial f(X)}{\partial x_\ell} \in \mathbb{R}^{n \times k_\ell}$ . Note we consider scalar outputs in this work, though the NFA relation is identical when there are  $c \geq 1$  outputs, where in this case  $\frac{\partial f(x)}{\partial x_\ell} \in \mathbb{R}^{k_\ell \times c}$  is the input-output Jacobian of the model  $f$ .

The NFA is equivalent to the statement that, for every layer  $\ell$ , the NFM  $F_\ell$  and AGOP  $\bar{G}_\ell$ , will have cosine similarity, or *correlation*,

$$\rho(F_\ell, \bar{G}_\ell) = 1,$$

where the correlation  $\rho$ , with range  $[-1, 1]$ , is defined as

$$\rho(A, B) = \text{tr}(A^\top B) \cdot \text{tr}(A^\top A)^{-1/2} \cdot \text{tr}(B^\top B)^{-1/2}.$$

for any two matrices  $A, B \in \mathbb{R}^{d_1 \times d_2}$ , for any  $d_1$  and  $d_2$ .

We note that while the NFA states exact proportionality, in practice, the NFM and AGOP are highly correlated with correlation less than 1 (see e.g. Figure 2), where the final correlation depends on many aspects of training and architecture choice. For example, the final value of the UC-NFA can be sensitive to the magnitude of the initial weights (e.g. first column of Figure 2). We parameterize this magnitude by the *initialization scale*,  $s_\ell$ , for layer  $\ell$ , where the initial weights are sampled i.i.d. as  $W_{ij}^{(\ell)} \sim \mathcal{N}\left(0, \frac{s_\ell}{k_\ell}\right)$ .

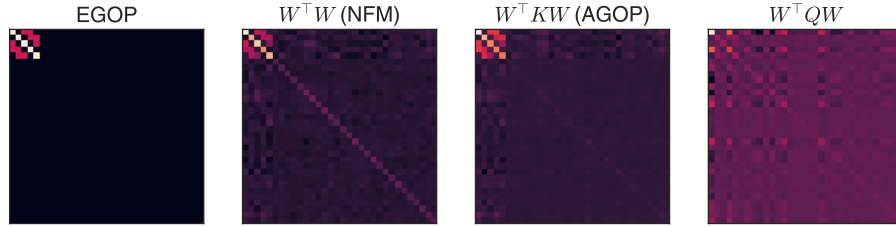


Figure 1. Various feature learning measures for target function  $y(x) = \sum_{k=1}^r x_{k \bmod r} \cdot x_{(k+1) \bmod r}$  with  $r = 5$  and inputs drawn from standard normal. The EGOP  $\mathbb{E}_{x \sim \mu} \left[ \frac{\partial y}{\partial x} \frac{\partial y}{\partial x}^\top \right]$  (first plot) captures the low-rank structure of the task. The NFM ( $W^\top W$ ) (second plot) and AGOP ( $W^\top K W$ ) (third plot) of a fully-connected network are similar to each other and the EGOP. Replacing  $K$  with a symmetric matrix  $Q$  with the same spectrum but independent eigenvectors obscures the low rank structure (fourth plot), and reduces the correlation from  $\rho(F, \bar{G}) = 0.93$  to  $\rho(F, W^\top Q W) = 0.53$ .

The relation between the NFM and the AGOP is significant, in part, because for a neural network that has learned enough information about the target function, the AGOP of this model with respect to the first-layer inputs will approximate the *expected gradient outer product* (EGOP) of the target function (Yuan et al., 2023). In particular, as we will see later with the example of a low rank polynomial, the EGOP of the target function contains task-specific structure that is completely independent of the model used to estimate it. Where the labels are generated from a particular target function  $y(x) : \mathbb{R}^d \rightarrow \mathbb{R}$  on data sampled from a distribution  $\mu$ , the EGOP is equal to,

$$\text{EGOP}(y, \mu) = \mathbb{E}_{x \sim \mu} \left[ \frac{\partial y}{\partial x} \frac{\partial y}{\partial x}^\top \right].$$

If the NFA holds, the correlation of the EGOP and the AGOP at the end of training also implies high correlation between the NFM of the first layer and the EGOP, so that the NFM has encoded this task-specific structure.

To demonstrate the significance of the approximate proportionality between the NFM and the AGOP in successfully trained networks, we return to the chain-monomial low rank task. In this case,  $\text{EGOP}(y, \mu)$  will be rank  $r$ , where  $r$  is much less than the ambient dimension (Figure 1). Similarly, the AGOP of the trained model resembles the EGOP. In this case the NFA implies that the NFM also resembles the EGOP. Therefore, the neural network has learned the model-independent and task-specific structure of the chain-monomial task in the right singular values and vectors of the first layer weight matrix, as these are determined by the NFM. As a demonstration of this fact, the NFM of a trained neural network can be recovered up to high correlation from the AGOP of a fixed kernel method on real datasets (Radhakrishnan et al., 2022)

This insight has inspired iterative kernel methods which can match the performance of fully-connected networks (Radhakrishnan et al., 2022; 2024) and can close the gap with

convolutional networks (Beaglehole et al., 2023). Additional prior works demonstrate the benefit of including the AGOP features to improve feature-less predictors (Hristache et al., 2001; Trivedi et al., 2014; Kpotufe et al., 2016). Additionally, because the NFM is correlated with the AGOP, the AGOP can be used to recover the features from feature-less methods, such as kernel machines.

## 2.2. Alignment decomposition

In order to understand the NFA, it is useful to decompose the AGOP. Doing so will allow us to show that the NFA can be interpreted as an alignment between weight matrices and the *pre-activation tangent kernel* (PTK), which is closely related to the *neural tangent kernel* (NTK).

For any layer  $\ell$ , we can re-write the AGOP as,

$$\bar{G}_\ell = (W^{(\ell)})^\top K^{(\ell)} W^{(\ell)}, \quad K^{(\ell)} \equiv \frac{\partial f(X)}{\partial h_\ell}^\top \frac{\partial f(X)}{\partial h_\ell}$$

This gives us the following proposition:

**Proposition 2** (Alignment decomposition of NFA).

$$\rho(F_\ell, \bar{G}_\ell) = \rho\left((W^{(\ell)})^\top W^{(\ell)}, (W^{(\ell)})^\top K^{(\ell)} W^{(\ell)}\right).$$

This alignment holds trivially and exactly if  $K^{(\ell)}$  is the identity. However, the correlation can be high in trained networks even with non-trivial  $K^{(\ell)}$ . For example, in the chain monomial task (Figure 1),  $K^{(0)}$  is far from identity (standard deviation of its eigenvalues is 5.9 times its average eigenvalue), but the NFA correlation is 0.93 at the end of training. We also note that if  $K^{(\ell)}$  is independent of  $W^{(\ell)}$ , the alignment is lower than in trained networks; in the same example, replacing  $K^{(0)}$  with a matrix  $Q$  with equal spectrum but random eigenvectors greatly reduces the correlation to 0.53 and qualitatively disrupts the structure relative to the NFM (Figure 1, rightmost column). We show the same result for the CelebA dataset (see Appendix K).

Therefore, the NFA has to do with the alignment of the left eigenvectors of  $W^{(\ell)}$  with  $K^{(\ell)}$  in addition to spectral considerations.

The  $k_\ell \times k_\ell$  matrix  $K^{(\ell)}$  is the feature covariance of the pre-activation tangent kernel (PTK)  $\mathcal{K}^{(\ell)}$  which we define as:

$$\mathcal{K}^{(\ell)}(x, z) \equiv \frac{\partial f(x)}{\partial h_\ell} \cdot \frac{\partial f(z)}{\partial h_\ell} \quad (2)$$

The PTK is related to the layerwise empirical NTK (ENTK)  $\hat{\Theta}_\ell$  by the following identity:

**Proposition 3** (Pre-activation to neural tangent identity). *Consider a depth- $L$  neural network  $f(x)$  with inputs  $X_\ell \in \mathbb{R}^{n \times k_\ell}$  to weight matrices  $W^{(\ell)} \in \mathbb{R}^{k_\ell \times k_\ell}$  for  $\ell \in [L]$ . Consider the empirical NTK where gradients are taken only with respect to  $W^{(\ell)}$  evaluated between two points  $x$  and  $z$  denoted by  $\hat{\Theta}_\ell(x_0, z_0) = \langle \frac{\partial f(x_0)}{\partial W^{(\ell)}}, \frac{\partial f(z_0)}{\partial W^{(\ell)}} \rangle$ . Then for all  $\ell$ ,  $\hat{\Theta}_\ell$  satisfies,*

$$\hat{\Theta}_\ell(x_0, z_0) = \mathcal{K}^{(\ell)}(x_0, z_0) \cdot x_\ell^\top z_\ell.$$

Therefore, the NFA is a statement about the alignment of the weight matrices with the PTK feature covariance - which itself is a factor of the layerwise NTK.

### 2.3. Centering the NFA isolates weight-PTK alignment

We showed that the NFA is equivalent to PTK-weight alignment (Proposition 2), and that it emerges during training (Figure 2 and Appendix G). We now ask: is the development of the NFA due to alignment of the weight matrices to the current PTK, or the alignment of the PTK to the current weights?

In practice, both effects matter, but numerical evidence suggests that changes in the PTK don't drive the early dynamics of the NFA (Appendix B). Instead, we focus on the alignment of the weights to the PTK at early times. We can measure this alignment using an alternative, centered version of the NFA:

**Ansatz 4** (Centered Neural Feature Ansatz). *Let  $W_0^{(\ell)}$ ,  $W^{(\ell)}$ , and  $K^{(\ell)}$  be the initial weight matrix, trained weight matrix, and interior feature matrix, respectively, at layer  $\ell$ , and let  $\bar{W}^{(\ell)} \equiv W^{(\ell)} - W_0^{(\ell)}$ . The centered neural feature ansatz (C-NFA) postulates that the following quantities will remain proportional to one another,*

$$(\bar{W}^{(\ell)})^\top \bar{W}^{(\ell)} \propto (\bar{W}^{(\ell)})^\top K^{(\ell)} \bar{W}^{(\ell)}.$$

We refer to the centered NFA as the C-NFA, and the original, uncentered NFA as the UC-NFA to distinguish them.

Since  $\bar{W} = 0$  at initialization, the early dynamics of the C-NFA are dominated by  $W$  aligning with the initial  $K$ :

**Proposition 5** (Centered NFA dynamics). *At initialization,  $\bar{W}^\top \bar{W} = \bar{W}^\top K \bar{W} = 0$ , and,*

$$\begin{aligned} \frac{d}{dt}(\bar{W}^\top \bar{W}) &= 0, & \frac{d^2}{dt^2}(\bar{W}^\top \bar{W}) &= 2\dot{W}^\top \dot{W}, \\ \frac{d}{dt}(\bar{W}^\top K \bar{W}) &= 0, & \frac{d^2}{dt^2}(\bar{W}^\top K \bar{W}) &= 2\dot{W}^\top K \dot{W}. \end{aligned}$$

The first non-zero derivatives of the two quantities in the C-NFA give us the change in the gram matrix of  $W$ , as well as the change in the AGOP for fixed PTK  $K$ . This makes it a useful object to study weight-PTK alignment.

We note that the C-NFA correlation remains high throughout training across initialization scale (Figure 2, second column, and Appendix G), but is especially high and invariant to scale early on in training. This is in contrast to the UC-NFA, whose final value can be extremely sensitive to the initialization scale (e.g. second row, Figure 2).

In the remainder of this work, we first analyze the C-NFA in early training and show that gradient based training drives the C-NFA, with a strength that depends on model and datasets. (Section 3). We then discuss initializations and optimizers which can increase the strength of the C-NFA and induce larger correlation between  $F$  and  $\bar{G}$  (Section 4).

## 3. Theoretically predicting the centered NFA

### 3.1. Early time C-NFA dynamics

To understand the dynamics of the weights aligning to the PTK, we compute the time derivatives of the C-NFA at initialization (Appendix A):

**Proposition 6** (Centered NFA decomposition). *For a fully-connected neural network at initialization, whose weights are trained with gradient descent on a loss function  $\mathcal{L}$ ,*

$$\dot{W}^\top \dot{W} = X^\top \dot{\mathcal{L}} \mathcal{K} \dot{\mathcal{L}} X, \quad \dot{W}^\top K \dot{W} = X^\top \dot{\mathcal{L}} \mathcal{K}^2 \dot{\mathcal{L}} X \quad (3)$$

where  $\dot{\mathcal{L}}$  is the  $n \times n$  diagonal matrix of logit derivatives

$$\dot{\mathcal{L}} \equiv \text{diag} \left( \frac{\partial \mathcal{L}}{\partial f} \right)$$

We immediately see from these equations how gradient-based training can drive the NFA. Even though the NFA doesn't explicitly involve the loss, the gradient descent dynamics of the NFM and AGOP depend on the labels in a similar way, and differ by a factor of the kernel  $\mathcal{K}$  - similar to how the AGOP and NFM differ by a factor of  $K$ .

When  $\mathcal{K}$  is proportional to a projection matrix, i.e.  $\mathcal{K} \propto \mathcal{K}^2$ , these derivatives will be perfectly correlated. Even in the general case where  $\mathcal{K}$  is dispersed with moderate eigenvalue decay, and does not commute with  $\dot{\mathcal{L}} X X^\top \dot{\mathcal{L}}$ , the two quantities have non-negative covariance. In the next section we



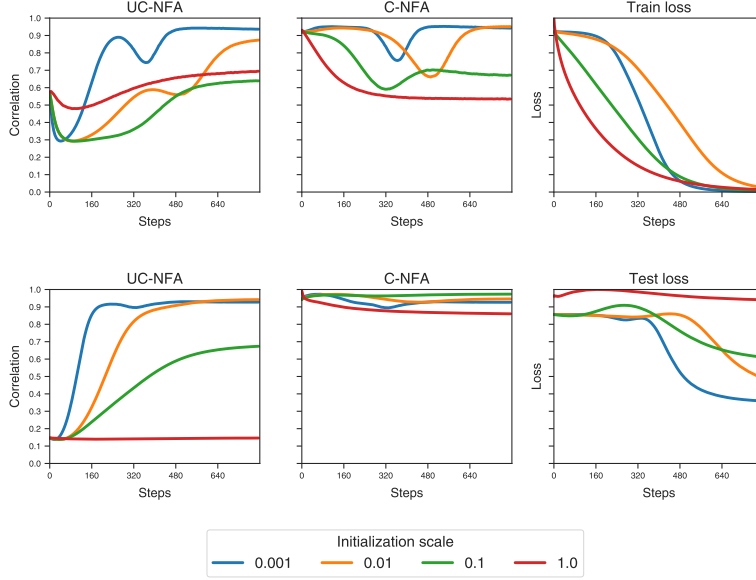


Figure 2. Uncentered and centered NFA correlations for a two hidden layer MLP trained on data drawn from a standard Normal distribution on the chain monomial task of rank  $r = 5$ . Only, the initialization scale of the first layer weights is varied, while  $s_\ell = 1$  for  $\ell > 0$ . The top row shows the values for layer 1, while the bottom row are the values for layer 2. Train (test) losses are scaled by the maximum train (test) loss achieved so that they are between 0 and 1. Here width is 256, the input dimension is 32, and the dataset contains 256 points.

will construct a dataset which interpolates between adversarial and aligned eigenstructure to demonstrate the range of possible values the derivative correlations can take.

In order to understand the correlation more quantitatively, we will focus on the case of mean-squared error (MSE) loss in the rest of this work. Here  $\hat{\mathcal{L}}$  corresponds to the diagonal matrix of the residuals  $y - f(x)$ . If the outputs of the network is 0 on the training data, then  $\hat{\mathcal{L}} = Y \equiv \text{diag}(y)$ , the labels themselves. In that case, the correlation of the time derivatives at initialization is a function of the input-label covariances as well as the PTK matrix:

$$\rho\left(\dot{W}^\top \dot{W}, \dot{W}^\top K \dot{W}\right) = \text{tr}\left(X^\top Y K Y X X^\top Y K^2 Y X\right) \cdot \text{tr}\left(\left(X^\top Y K Y X\right)^2\right)^{-1/2} \cdot \text{tr}\left(\left(X^\top Y K^2 Y X\right)^2\right)^{-1/2} \quad (4)$$

In general we expect that these quantities can self-average under the appropriate high-dimensional limits. It is helpful then to write down the average (over initializations) of the covariance. Taking expectation of the first factor,

$$\begin{aligned} \mathbb{E}\left[\text{tr}\left(X^\top Y K Y X X^\top Y K^2 Y X\right)\right] = \\ \text{tr}\left(X^\top Y \mathbb{E}[K] Y X X^\top Y \mathbb{E}[K^2] Y X\right) \\ + \text{tr}\left(\text{Cov}\left(X^\top Y K Y X, X^\top Y K^2 Y X\right)\right) \end{aligned} \quad (5)$$

A similar decomposition exist for the denominator terms.

The simplest limit is the NTK regime where the width tends to infinity with fixed number of data points and input dimension. Here the PTK matrix will approach its expectation, and the second, covariance term above will tend to 0. This suggests that the first (mean) term encodes much of the interesting phenomenology near initialization for large networks. We use this fact to design a dataset that interpolates between small and large initial derivatives of the C-NFA, even in the non-NTK regime, which will help us demonstrate the validity of our random matrix theory approach.

We focus most of our random matrix theory analysis on a one-hidden layer network, as the calculations quickly become complicated with depth. However, we also show that the mean term can be used to approximately predict the NFA value for Gaussian data with different spectral decay rates for more complicated networks (see Appendix C).

### 3.2. Exact predictions with one hidden layer, quadratic activation

We can capture the behavior of both the mean and covariance terms from Equation (5) in certain high dimensional settings. In particular for one hidden layer neural networks with quadratic activations, we can exactly predict the value of Equation (5) in the high dimensional limit. We make the assumption that  $X$  and  $Y$  are (asymptotically) freely independent of the parameters at initialization, and that the resulting average is close to the value of any specific network initialization (self-averaging). For more details on the

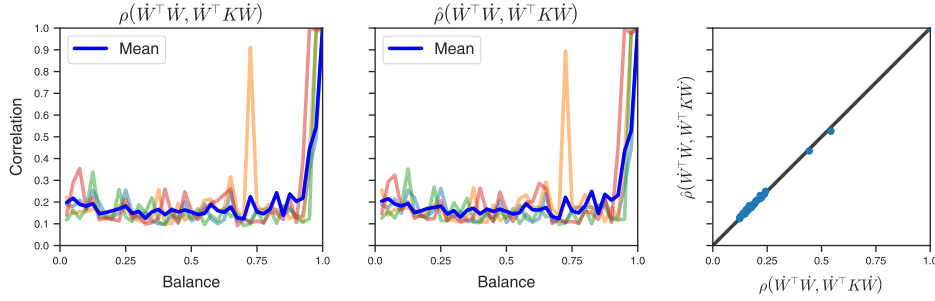


Figure 3. Predicted versus observed correlation of the second derivatives of centered  $F$  and  $\bar{G}$  on the alignment reversing dataset. Different shaded color curves correspond to four different seeds for the dataset. The solid blue curve is the average over all data seeds. The rightmost sub-figure is a scatter plot of the predicted versus observed correlations of these second derivatives, with one point for each balance value. We instantiate the dataset in the proportional regime where width, input dimension, and dataset size are all equal to 1024.

assumptions, see Appendix E. We then show numerically that the predicted correlation between the second derivatives of the centered NFM and AGOP matches the observed correlation across individual random instances of the dataset.

To illustrate our analysis, we derive here the numerator of Equation (4). Let  $M_{X|Y}^{(4)} = (X^\top Y X)^2$ , and  $M_X^{(2)} = X^\top X$ , and  $F_a = W^\top \text{diag}(a^2) W$ . Then,

$$\begin{aligned} & \text{tr}(X^\top Y \mathcal{K} Y X X^\top Y \mathcal{K}^2 Y X) \\ &= \text{tr}\left(M_{X|Y}^{(4)} F_a M_{X|Y}^{(4)} F_a M_X^{(2)} F_a\right). \end{aligned}$$

We can simplify this alternating product using standard results from random matrix theory, and factor the parameter and data contributions at the cost of increasing the number of terms in the expression (Appendix E).

In the simplified case of isotropic data  $X^\top X = I$ , we have:

$$\begin{aligned} & \text{tr}(X^\top Y \mathcal{K} Y X X^\top Y \mathcal{K}^2 Y X) \\ &= \text{tr}\left(M_{X|Y}^{(4)}\right)^2 \text{tr}(F_a^3) + \text{tr}(F_a) \text{tr}(F_a^2) \text{tr}\left(\left(\bar{M}_{X|Y}^{(4)}\right)^2\right). \end{aligned}$$

From these random matrix calculations, we see that the correlations of the derivatives are determined by traces of powers of  $M_{X|Y}^{(4)}$  (and  $M_X^{(2)}$  by the calculations in Section E), which is specific to the dataset, and  $F_a$ , which is specific to the architecture and initialization.

**Manipulating the C-NFA** To numerically explore the validity of the random matrix theory calculations, we need a way to generate datasets with different values of  $\rho(\dot{W}^\top \dot{W}, \dot{W}^\top \mathcal{K} \dot{W})$ . We construct a random dataset called the *alignment reversing* dataset, parameterized by a *balance* parameter  $\gamma \in (0, 1]$  to adversarially disrupt the NFA near initialization in the regime that width  $k$ , input dimension  $d$ , and dataset size  $n$  are all equal ( $n = k = d = 1024$ ). By Proposition 12, for the aforementioned

neural architecture, the expected second derivative of the centered NFM satisfies,  $\mathbb{E}[\dot{W}^\top \dot{W}] = X^\top Y \mathbb{E}[\mathcal{K}] Y X = (X^\top Y X)^2$ , while the expected second derivative of the centered AGOP,  $\mathbb{E}[\dot{W}^\top \mathcal{K} \dot{W}] = X^\top Y \mathbb{E}[\mathcal{K}^2] Y X$ , has an additional component  $X^\top Y X \cdot X^\top X \cdot X^\top Y X$ . Our construction exploits this difference in that  $X^\top X$  becomes adversarially unaligned to  $X^\top Y X$  as the balance parameter decreases. In our experiment, we sample multiple random datasets with this construction and compute the predicted and observed correlation of the second derivatives of the centered NFA at initialization.

The construction exploits that we can manipulate  $X^\top Y X \cdot X^\top X \cdot X^\top Y X$  freely of the NFM using a certain choice of  $Y$  (see Appendix F for details of the construction). We design the dataset such that this AGOP-unique term is close to identity, while the NFM second derivative has many large off-diagonal entries, leading to low correlation between the second derivatives of the NFM and AGOP.

We observe in Figure 3 that the centered NFA correlations predicted with random matrix theory closely match the observed values, across individual four random seeds and for the average of the correlation across them. Crucially, a single neural network is used across the datasets, confirming the validity of the self-averaging assumption. The variation in the plot across seeds come from randomness in the sample of the data, which cause deviations from the adversarial construction.

#### 4. Increasing the centered contribution to the uncentered NFA improves feature learning

Our theoretical and experimental work has established that gradient based training leads to alignment of the weight matrices to the PTK feature covariance. This process is driven by the C-NFA. Therefore, one path

towards improving the correlations defined by the NFA is to increase the contribution of the C-NFA to the dynamics - as measured, for example, by the ratio  $\text{tr}(\bar{W}^\top \bar{W} \bar{W}^\top K \bar{W}) \text{tr}(W^\top W W^\top K W)^{-1}$ . When this ratio is large, the C-NFA contributes significantly in magnitude to the UC-NFA, indicating successful feature learning. We will discuss two interventions which increase this ratio, with an eye towards improving generalization.

#### 4.1. Feature learning and initialization

One factor that modulates the level of feature learning is the scale of the initialization in each layer. In our experiments training networks with unmodified gradient descent, we observe that the centered NFA will increasingly dominate the uncentered NFA with decreasing initialization (third panel, first row, Figure 4). Further, as the centered NFA increases in contribution to the uncentered quantity, the strength of the UC-NFA, and to a lesser extent, the C-NFA increases (Figure 4). The decreases in correspondence between these quantities is also associated with a decrease in the feature quality of the NFM (Appendix H) and test error (Figure 2) for the chain monomial task.

For fully-connected networks with homogeneous activation functions, such as ReLU, and no normalization layers, decreasing initialization scale is equivalent to decreasing the scale of the outputs, since we can write  $f(Wx) = a^{-p} f(aWx)$  for any scalar  $a$  for any homogenous activation  $f$ . This in turn is equivalent to increasing the scale of the labels. Therefore, decreasing initialization forces the weights to change more in order to fit the labels, leading to more change in  $F$  from its initialization. Conceptually, this aligns with the substantial line of empirical and theoretical evidence that increasing initialization scale or output scaling transitions training between the lazy and feature learning regimes (Chizat et al., 2019; Woodworth et al., 2020; Agarwala et al., 2020; Lyu et al., 2023).

This relationship suggests that small initialization can be broadly applied to increase the change in  $F$ , and the strength of the UC-NFA. However, this may not be ideal; for example, if the activation function is differentiable at 0, small initialization leads to a network which is approximately linear. This may lead to low expressivity unless the learning dynamics can increase the weight magnitude.

#### 4.2. Speed Limited Optimization

We can instead design an intervention which can increase feature learning without the need to decrease the initialization scale. We do so by fixing the learning *speed* layerwise to constant values, which causes the C-NFA to dominate the UC-NFA dynamics. For weights at layer  $\ell$  and learning rate  $\eta > 0$ , we introduce *Speed Limited Optimization (SLO)*,

which is characterized by the following update rule,

$$W_{t+1}^{(\ell)} \leftarrow W_t^{(\ell)} + \eta \cdot C_\ell \cdot \frac{\nabla_{W_t^{(\ell)}} \mathcal{L}}{\|\nabla_{W_t^{(\ell)}} \mathcal{L}\|}$$

where the hyperparameter  $C_\ell \geq 0$  controls the amount of learning in layer  $\ell$ . We expect this rule to increase the strength of the UC-NFA in layers where  $C_\ell$  is large relative to  $C_m$  for  $m \neq \ell$ , as  $W^{(\ell)}$  will be forced to change significantly from initialization. As a result,  $\|W_0^{(\ell)}\| \left\| W_t^{(\ell)} \right\|^{-1} \rightarrow 0$  for large  $t$ , causing the centered and uncentered NFA to coincide for this layer.

We demonstrate the effects of SLO on the chain-monomial task (Equation (1)). We found that fixing the learning speed to be high in the first layer and low in the remaining layers causes the ratio of the unnormalized C-NFA to the UC-NFA to become close to 1 across initialization scales (Figure 4b). The same result holds for the SVHN dataset (see Appendix K). We note that this intervention can be applied to target underperforming layers and improve generalization in deeper networks (see Appendix J for details).

We observe that the correlations from both the C-NFA and the UC-NFA become close to 1 after training with SLO, independent of initialization scale (Appendix H). Further, the quality of the features learned, measured by the similarity of  $F$  and  $\bar{G}$  to the true EGOP, significantly improve and are more similar to each other with SLO (Figure 5), even with large initialization. In contrast, in standard training the UC-NFA fails to develop with large initialization, as  $F$  resembles identity (no feature learning), while  $\bar{G}$  only slightly captures the relevant features.

## 5. Discussion

**Centered NFA through training** Our theoretical analysis in this work shows that the PTK feature covariance at initialization has a relatively simple structure in terms of the weights and the data. To predict the correlation of the NFA later in training, we will likely need to account for the change in this matrix. One should be able to predict this development at short times by taking advantage of the fact that eigenvectors of the Hessian change slowly during training (Bao et al., 2023). An alternative approach would be to use a quadratic model for neural network dynamics (Agarwala et al., 2022; Zhu et al., 2022) which can capture dynamics of the NTK (and therefore the PTK).

**Depth and general activations** We provide an analytic prediction for the C-NFA at initialization for one hidden layer networks with quadratic activation functions, and provide first-order predictions for two hidden layer networks with quadratic and ReLU activations. A followup direction would be to use random matrix analysis to more accurately

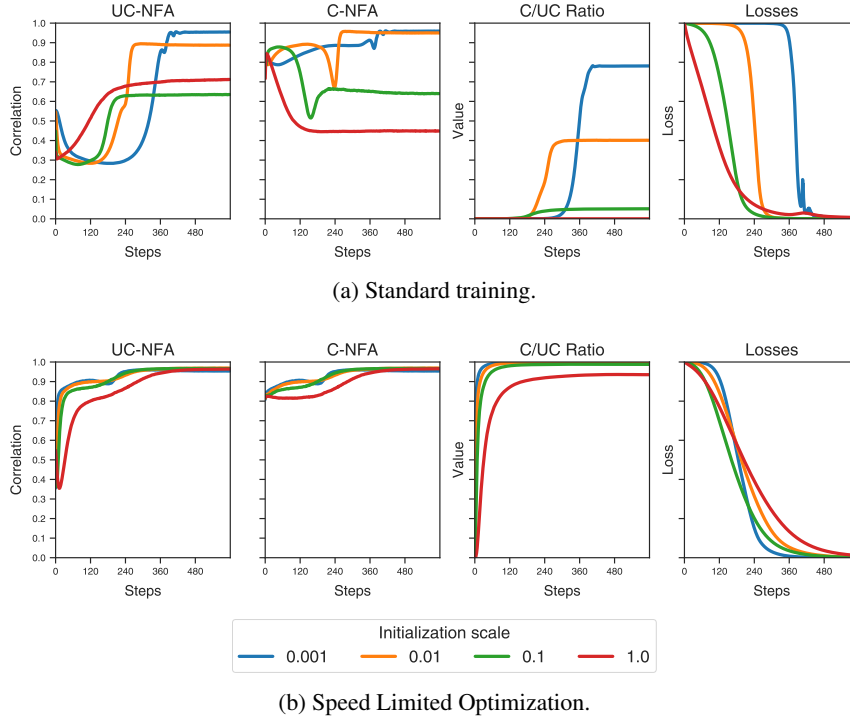


Figure 4. The uncentered and centered NFA for the first layer weight matrix as a function of initialization, with and without SLO. We consider a two hidden layer network with ReLU activations, where we set  $C_0 = 500$ , and  $C_1 = C_2 = 0.002$ . The third column shows the ratio of the unnormalized C-NFA correlation to the UC-NFA:  $\text{tr}(\bar{W}^\top \bar{W} \bar{W}^\top K \bar{W}) \cdot \text{tr}(W^\top W W^\top K W)^{-1}$ . We show that SLO pushes the ratio of the unnormalized C-NFA to UC-NFA close to 1 and improves the UC-NFA across initialization scales.

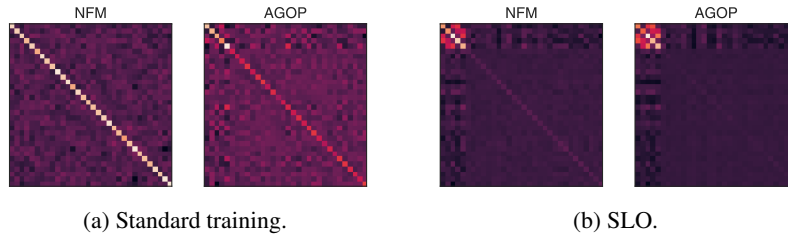


Figure 5. The NFM and AGOP from a trained network with and without Speed Limited Optimization with fixed initialization scale on the chain monomial task. With standard training and large initialization, the NFM remains close to identity, and does not learn task structure. SLO increases feature learning, causing the NFM to become highly correlated with the AGOP and learn the target features.

predict the NFA for deep architectures with general activations. A promising approach in this direction is to approximate non-linear activations with a linear expansion and independent correction terms (Adlam et al., 2019; Adlam and Pennington, 2020; El Karoui, 2008; Hu and Lu, 2022).

More generally it’s an open question as to how the NFA develops with depth in more complicated architectures like CNNs and transformers. More research is needed to understand how PTK-weight alignment relates to generalization and trainability in deep networks.

**Speed Limited Optimization** There are prior works that implement differential learning rates across layers (Howard and Ruder, 2018; Singh et al., 2015), though these differ from differential learning *speeds* as in SLO, in which the L2-norm of the gradients are fixed, and not the scaling of the gradients. Our intervention is more similar to the LARS (You et al., 2017) and LAMB (You et al., 2019) optimizers that fix learning speeds to decrease training time in ResNet and BERT architectures. However, these optimizers fix learning speeds to the norm of the weight matrices, while our intervention sets learning speeds to free hyperparameters in order to increase feature learning, as measured by the NFA.



We also note as an additional explanation for the success of SLO in our experiments, the PTK feature covariance may change slowly (or just in a single direction) with this optimizer, because the learning rate is small for later layers, allowing the first layer weights to align with the PTK.

**Adaptive and stochastic optimizers** We demonstrate in this work that the dataset (by our construction in Section 3) and optimizer (with SLO in Section 4) play a significant role in the strength of feature learning. Important future work would be to understand other settings where significant empirical differences exist between optimization choices. In particular, analyzing the NFA may clarify the role of gradient batch size and adaptive gradient methods in generalization (Zhu et al., 2023).

## 6. Acknowledgements

We thank Lechao Xiao for detailed feedback on the manuscript. We also thank Jeffrey Pennington for helpful discussions.

## References

- Emmanuel Abbe, Enric Boix Adsera, and Theodor Misiakiewicz. The merged-staircase property: a necessary and nearly sufficient condition for sgd learning of sparse functions on two-layer neural networks. In *Conference on Learning Theory*, 2022.
- Ben Adlam and Jeffrey Pennington. The neural tangent kernel in high dimensions: Triple descent and a multi-scale theory of generalization. In *International Conference on Machine Learning*, pages 74–84. PMLR, 2020.
- Ben Adlam, Jake Levinson, and Jeffrey Pennington. A random matrix perspective on mixtures of nonlinearities for deep learning. *arXiv preprint arXiv:1912.00827*, 2019.
- Atish Agarwala, Jeffrey Pennington, Yann Dauphin, and Sam Schoenholz. Temperature check: theory and practice for training models with softmax-cross-entropy losses. *arXiv preprint arXiv:2010.07344*, 2020.
- Atish Agarwala, Fabian Pedregosa, and Jeffrey Pennington. Second-order regression models exhibit progressive sharpening to the edge of stability. *arXiv preprint arXiv:2210.04860*, 2022.
- Zeyuan Allen-Zhu and Yuanzhi Li. What Can ResNet Learn Efficiently, Going Beyond Kernels? In *Advances in Neural Information Processing Systems*, 2019.
- Jimmy Ba, Murat A Erdogdu, Taiji Suzuki, Zhichao Wang, Denny Wu, and Greg Yang. High-dimensional Asymptotics of Feature Learning: How One Gradient Step Improves the Representation. *arXiv preprint arXiv:2205.01445*, 2022.
- Xuchan Bao, Bietti Alberto, Aaron Defazio, and Vivien Cabannes. Hessian inertia in neural networks. *1st Workshop on High-dimensional Learning Dynamics*, 2023.
- Boaz Barak, Benjamin L Edelman, Surbhi Goel, Sham Kakade, Eran Malach, and Cyril Zhang. Hidden progress in deep learning: Sgd learns parities near the computational limit. *arXiv preprint arXiv:2207.08799*, 2022.
- Daniel Beaglehole, Adityanarayanan Radhakrishnan, Parthe Pandit, and Mikhail Belkin. Mechanism of feature learning in convolutional neural networks. *arXiv preprint arXiv:2309.00570*, 2023.
- Tom Brown, Benjamin Mann, Nick Ryder, Melanie Subbiah, Jared D Kaplan, Prafulla Dhariwal, Arvind Neelakantan, Pranav Shyam, Girish Sastry, Amanda Askell, et al. Language models are few-shot learners. *Advances in neural information processing systems*, 33:1877–1901, 2020.
- Lenaic Chizat, Edouard Oyallon, and Francis Bach. On lazy training in differentiable programming. *Advances in neural information processing systems*, 32, 2019.
- Alexandru Damian, Jason Lee, and Mahdi Soltanolkotabi. Neural networks can learn representations with gradient descent. In *Conference on Learning Theory*, pages 5413–5452. PMLR, 2022.
- Noureddine El Karoui. Spectrum estimation for large dimensional covariance matrices using random matrix theory. 2008.
- B. Ghorbani, Song Mei, Theodor Misiakiewicz, and Andrea Montanari. Limitations of Lazy Training of Two-layers Neural Networks. In *Advances in Neural Information Processing Systems*, 2019.
- Jeremy Howard and Sebastian Ruder. Universal language model fine-tuning for text classification. *arXiv preprint arXiv:1801.06146*, 2018.
- Marian Hristache, Anatoli Juditsky, Jorg Polzehl, and Vladimir Spokoiny. Structure adaptive approach for dimension reduction. *Annals of Statistics*, pages 1537–1566, 2001.
- Hong Hu and Yue M Lu. Universality laws for high-dimensional learning with random features. *IEEE Transactions on Information Theory*, 69(3):1932–1964, 2022.
- Arthur Jacot, Franck Gabriel, and Clement Hongler. Neural Tangent Kernel: Convergence and Generalization in Neural Networks. In *Advances in Neural Information Processing Systems*, 2018.

- Guangda Ji and Zhanxing Zhu. Knowledge distillation in wide neural networks: Risk bound, data efficiency and imperfect teacher. In *Advances in Neural Information Processing Systems*, 2020.
- Samory Kpotufe, Abdeslam Boularias, Thomas Schultz, and Kyoungok Kim. Gradients weights improve regression and classification. *Journal of Machine Learning Research*, 2016.
- Alex Krizhevsky, Ilya Sutskever, and Geoffrey E Hinton. Imagenet classification with deep convolutional neural networks. *Advances in neural information processing systems*, 25, 2012.
- Yuanzhi Li, Tengyu Ma, and Hongyang R Zhang. Learning over-parametrized two-layer neural networks beyond NTK. In *Conference on Learning Theory*, 2020.
- Kaifeng Lyu, Jikai Jin, Zhiyuan Li, Simon S Du, Jason D Lee, and Wei Hu. Dichotomy of early and late phase implicit biases can provably induce grokking. *arXiv preprint arXiv:2311.18817*, 2023.
- Ben Mildenhall, Pratul P Srinivasan, Matthew Tancik, Jonathan T Barron, Ravi Ramamoorthi, and Ren Ng. Nerf: Representing scenes as neural radiance fields for view synthesis. *Communications of the ACM*, 65(1):99–106, 2021.
- Behrad Moniri, Donghwan Lee, Hamed Hassani, and Edgar Dobriban. A theory of non-linear feature learning with one gradient step in two-layer neural networks. *arXiv preprint arXiv:2310.07891*, 2023.
- Alireza Mousavi-Hosseini, Sejun Park, Manuela Girotti, Ioannis Mitliagkas, and Murat A Erdogdu. Neural networks efficiently learn low-dimensional representations with sgd. *arXiv preprint arXiv:2209.14863*, 2022.
- Eshaan Nichani, Alex Damian, and Jason D Lee. Provable guarantees for nonlinear feature learning in three-layer neural networks. *arXiv preprint arXiv:2305.06986*, 2023.
- Suzanna Parkinson, Greg Ongie, and Rebecca Willett. Linear neural network layers promote learning single-and multiple-index models. *arXiv preprint arXiv:2305.15598*, 2023.
- Adityanarayanan Radhakrishnan, Daniel Beaglehole, Parthe Pandit, and Mikhail Belkin. Feature learning in neural networks and kernel machines that recursively learn features. *arXiv preprint arXiv:2212.13881*, 2022.
- Adityanarayanan Radhakrishnan, Mikhail Belkin, and Dmitriy Drusvyatskiy. Linear recursive feature machines provably recover low-rank matrices, 2024.
- Maria Refinetti, Sebastian Goldt, Florent Krzakala, and Lenka Zdeborová. Classifying high-dimensional Gaussian mixtures: Where kernel methods fail and neural networks succeed. In *International Conference on Machine Learning*, 2021.
- Karen Simonyan and Andrew Zisserman. Very deep convolutional networks for large-scale image recognition. *arXiv preprint arXiv:1409.1556*, 2014.
- Bharat Singh, Soham De, Yangmuzi Zhang, Thomas Goldstein, and Gavin Taylor. Layer-specific adaptive learning rates for deep networks. In *2015 IEEE 14th International Conference on Machine Learning and Applications (ICMLA)*, pages 364–368. IEEE, 2015.
- Shubhendu Trivedi, Jialei Wang, Samory Kpotufe, and Gregory Shakhnarovich. A consistent estimator of the expected gradient outerproduct. In *UAI*, pages 819–828, 2014.
- Blake Woodworth, Suriya Gunasekar, Jason D Lee, Edward Moroshko, Pedro Savarese, Itay Golan, Daniel Soudry, and Nathan Srebro. Kernel and rich regimes in over-parametrized models. In *Conference on Learning Theory*, pages 3635–3673. PMLR, 2020.
- Gilad Yehudai and Ohad Shamir. On the Power and Limitations of Random Features for Understanding Neural Networks. In *Advances in Neural Information Processing Systems*, 2019.
- Yang You, Igor Gitman, and Boris Ginsburg. Large batch training of convolutional networks. *arXiv preprint arXiv:1708.03888*, 2017.
- Yang You, Jing Li, Sashank Reddi, Jonathan Hseu, Sanjiv Kumar, Srinadh Bhojanapalli, Xiaodan Song, James Demmel, Kurt Keutzer, and Cho-Jui Hsieh. Large batch optimization for deep learning: Training bert in 76 minutes. *arXiv preprint arXiv:1904.00962*, 2019.
- Gan Yuan, Mingyue Xu, Samory Kpotufe, and Daniel Hsu. Efficient estimation of the central mean subspace via smoothed gradient outer products. *arXiv preprint arXiv:2312.15469*, 2023.
- Chiyuan Zhang, Samy Bengio, Moritz Hardt, Benjamin Recht, and Oriol Vinyals. Understanding deep learning (still) requires rethinking generalization. *Communications of the ACM*, 2021.
- Libin Zhu, Chaoyue Liu, Adityanarayanan Radhakrishnan, and Mikhail Belkin. Quadratic models for understanding neural network dynamics. *arXiv preprint arXiv:2205.11787*, 2022.

Libin Zhu, Chaoyue Liu, Adityanarayanan Radhakrishnan, and Mikhail Belkin. Catapults in sgd: spikes in the training loss and their impact on generalization through feature learning. *arXiv preprint arXiv:2306.04815*, 2023.

## A. Omitted proofs of propositions in the main text

*Proof of Proposition 3.* Note that  $\frac{\partial f(x_0)}{\partial \bar{W}^{(\ell)}} = \frac{\partial f(x_0)}{\partial h_\ell} x_0^\top \in \mathbb{R}^{k_\ell \times k_\ell}$ . Then,

$$\begin{aligned} \hat{\Theta}_\ell(x_0, z_0) &= \text{tr} \left( \frac{\partial f(x_0)}{\partial h_\ell} x_\ell^\top z_\ell \frac{\partial f(z_0)}{\partial h_\ell}^\top \right) \\ &= \frac{\partial f(x_0)}{\partial h_\ell}^\top \frac{\partial f(z_0)}{\partial h_\ell} \cdot x_\ell^\top z_\ell \\ &= \mathcal{K}^{(\ell)}(x_0, z_0) \cdot x_\ell^\top z_\ell. \end{aligned}$$

□

*Proof of Proposition 6.* At initialization, we have,  $\dot{W} = \frac{\partial f(X)}{\partial h_1}^\top \dot{L}X$ . Therefore, using that  $\mathcal{K} \equiv \frac{\partial f(X)}{\partial h_1} \frac{\partial f(X)}{\partial h_1}^\top$ ,

$$\dot{W}^\top \dot{W} = X^\top \dot{L} \frac{\partial f(X)}{\partial h_1} \frac{\partial f(X)}{\partial h_1}^\top \dot{L}X = X^\top \dot{L} \mathcal{K} \dot{L}X,$$

and,

$$\begin{aligned} \dot{W}^\top K \dot{W} &= X^\top \dot{L} \frac{\partial f(X)}{\partial h_1} K \frac{\partial f(X)}{\partial h_1}^\top \dot{L}X \\ &= X^\top \dot{L} \frac{\partial f(X)}{\partial h_1} \frac{\partial f(X)}{\partial h_1}^\top \frac{\partial f(X)}{\partial h_1} \frac{\partial f(X)}{\partial h_1}^\top \dot{L}X \\ &= X^\top \dot{L} \mathcal{K}^2 \dot{L}X. \end{aligned}$$

□

## B. Additional centerings of the NFA

**Double-centered NFA** One may additionally center the PTK feature map to understand the co-evolution of the PTK feature covariance and the weight matrices. In this work, we consider such a centering that we refer to as the *double-centered* NFA.

**Ansatz 7** (Double-centered NFA).

$$(\bar{W}^{(\ell)})^\top \bar{W}^{(\ell)} \propto (\bar{W}^{(\ell)})^\top \bar{K}^{(\ell)} \bar{W}^{(\ell)},$$

where  $\bar{K}^{(\ell)} = \left( \frac{\partial f(X)}{\partial h_\ell} - \frac{\partial f_0(X)}{\partial h_\ell} \right)^\top \left( \frac{\partial f(X)}{\partial h_\ell} - \frac{\partial f_0(X)}{\partial h_\ell} \right)$ , and  $f_0$  is the neural network at initialization.

However, the double-centered NFA term corresponds to higher-order dynamics that do not significantly contribute the centered and uncentered NFA (Figure 6) when initialization is large or for early periods of training. Note however this term becomes relevant over longer periods of training.

**Isolating alignment of the PTK to the initial weight matrix** One may also center just the PTK feature map, while substituting the initial weights for  $W$  to isolate how the PTK feature covariance aligns to the weight matrices. To measure this alignment, we consider the *PTK-centered* NFA.

**Ansatz 8** (PTK-centered NFA).

$$(W_0^{(\ell)})^\top W_0^{(\ell)} \propto (W_0^{(\ell)})^\top \bar{K}^{(\ell)} W_0^{(\ell)},$$

where  $W_0^{(\ell)}$  is the initial weight matrix at layer  $\ell$ .

However, this correlation decreases through training, indicating that the correlation of these quantities does not drive alignment between the uncentered NFM and AGOP (Figure 7).

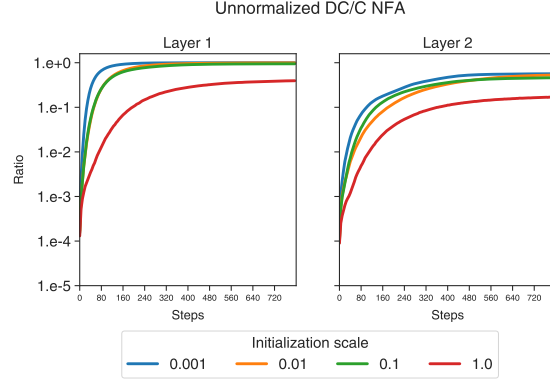


Figure 6. Ratio of the unnormalized double-centered NFA correlation to the centered NFA correlation throughout neural network training. In particular, we plot  $\text{tr}(\bar{W}^\top \bar{W} \bar{W}^\top \bar{K} \bar{W}) \cdot \text{tr}(\bar{W}^\top \bar{W} \bar{W}^\top K \bar{W})^{-1}$  throughout training for both layers of a two-hidden layer MLP with ReLU activations.

### C. Extending our theoretical predictions to depth and general activations

Precise predictions of the C-NFA become more complicated with additional depth and general activation functions. However, we note that the deep C-NFA will remain sensitive to a first-order approximation in which  $K$  is replaced by its expectation. We demonstrate that this term qualitatively captures the behavior of the C-NFA for 2 hidden layer architectures with quadratic and, to a lesser extent, ReLU activation functions in Figure 8. In this experiment, we sample Gaussian data with mean 0 and covariance with a random eigenbasis. We parameterize the eigenvalue decay of the covariance matrix by a parameter  $\alpha$ , called the data decay rate, so that the eigenvalues have values  $\lambda_k = \frac{1}{1+k^\alpha}$ . As  $\alpha$  approaches 0 or  $\infty$  the data covariance approaches a projector matrix.

In this experiment, we see that the data covariance spectrum will also parameterize the eigenvalue decay of  $\mathbb{E}[K]$ , allowing us to vary how close the expected PTK matrix (and its dual, the PTK feature covariance) is from a projector, where the NFA holds exactly. We see that for intermediate values of  $\alpha$ , both the observed and the predicted derivatives of the C-NFA decreases in value.

We plot the observed values in two settings corresponding to different asymptotic regimes. One setting is the proportional regime, where  $n = k = d = 128$ . The other is the NTK regime where  $n = d = 128$  and  $k = 1024$ . For the quadratic case, as the network approaches infinite width, the prediction more closely matches the observed values. Additional terms corresponding to the nonlinear part of  $\phi'$  in ReLU networks, the derivative of the activation function, are required to capture the correlation more accurately in this case.

### D. Proofs and derivations

*Proof of Proposition 5.* Consider the second derivatives of the NFM and the AGOP.

$$\frac{d}{dt}(\bar{W}^\top \bar{W}) = \dot{W}^\top \bar{W} + \bar{W}^\top \dot{W}.$$

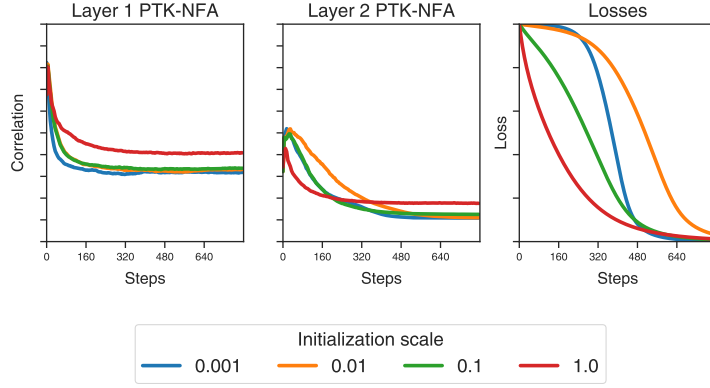
Then,

$$\frac{d^2}{dt^2}(\bar{W}^\top \bar{W}) = 2\dot{W}^\top \dot{W} + \ddot{W}^\top \bar{W} + \bar{W}^\top \ddot{W}.$$

At initialization  $\bar{W} = 0$ , therefore,

$$\bar{W}^\top \bar{W} = 0, \quad \frac{d}{dt}(\bar{W}^\top \bar{W}) = 0, \quad \frac{d^2}{dt^2}(\bar{W}^\top \bar{W}) = 2\dot{W}^\top \dot{W}. \quad (6)$$





(a) Isotropic data.

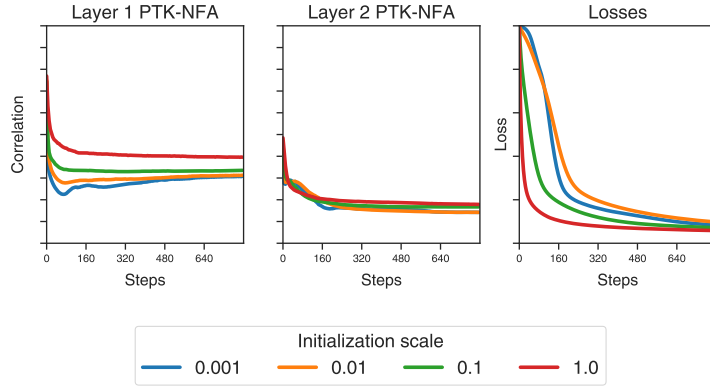

 (b) Data spectrum with decay  $\lambda_k \sim \frac{1}{1+k^2}$ .

Figure 7. PTK-centered NFA correlation throughout training for both layers of a two-hidden layer MLP with ReLU activations on Gaussian data with two different spectra.

Meanwhile, for the (centered) AGOP,

$$\frac{d}{dt}(\bar{W}^\top K \bar{W}) = \dot{W}^\top K \bar{W} + \bar{W}^\top \dot{K} \bar{W} + \bar{W}^\top K \dot{W}.$$

Then,

$$\begin{aligned} \frac{d^2}{dt^2}(\bar{W}^\top K \bar{W}) &= \ddot{W}^\top K \bar{W} + \dot{W}^\top \dot{K} \bar{W} + \dot{W}^\top K_z \dot{W} \\ &\quad + \dot{W}^\top K \dot{W} + \bar{W}^\top \dot{K} \dot{W} + \bar{W}^\top K \ddot{W} \\ &\quad + \dot{W}^\top \dot{K} \bar{W} + \bar{W}^\top \ddot{K} \bar{W} + \bar{W}^\top \dot{K} \dot{W}. \end{aligned}$$

At initialization,

$$\bar{W}^\top K \bar{W} = 0, \quad \frac{d}{dt}(\bar{W}^\top K \bar{W}) = 0, \tag{7}$$

$$\frac{d^2}{dt^2}(\bar{W}^\top K \bar{W}) = 2\dot{W}^\top K \dot{W}. \tag{8}$$

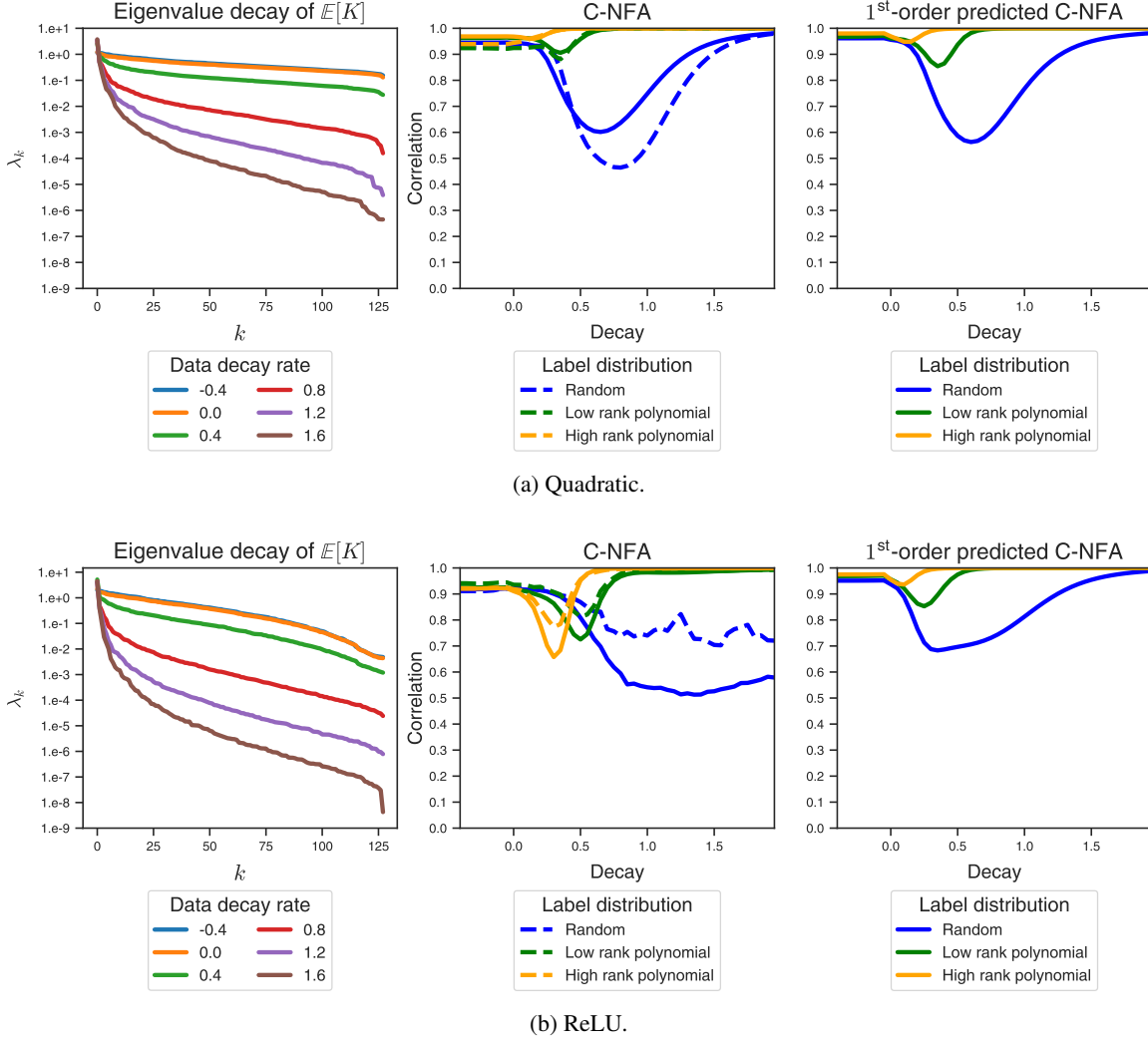


Figure 8. Observed versus the first-order predicted C-NFA for the input to the first layer of a two hidden layer MLP. The dashed line is neural network width  $k = n = d = 128$ , where  $n$  and  $d$  are the number of data point and data dimension, respectively, while the solid line uses  $n = d = 128$  and  $k = 1024$ .

Therefore, the correlation between the centered neural feature matrix and the centered AGOP at initialization is determined by,

$$\rho(\dot{W}^\top \dot{W}, \dot{W}^\top K \dot{W}) .$$

Both sides simplify at initialization:

$$\dot{W}^\top \dot{W} = X^\top Y K Y X, \quad \dot{W}^\top K \dot{W} = X^\top Y K^2 Y X ,$$

where  $K$  is its value at initialization. □

## E. Free probability calculations of C-NFA

In order to understand the development of the NFA, we analyze the centered NFA in the limit that learning rate is much smaller than the initialization for a one hidden layer MLP with quadratic activations. We write this particular network as,

$$f(x) = a^\top (Wx)^2 ,$$

where  $a \in \mathbb{R}^{1 \times k}$  and  $W \in \mathbb{R}^{k \times d}$ , where  $d$  is the input dimension and  $k$  is the width. In this case, the NFA has the following form,

$$\rho(F, \bar{G}) = \frac{\text{tr}(X^\top Y \mathcal{K} Y X X^\top Y \mathcal{K}^2 Y X)}{\text{tr}((X^\top Y \mathcal{K} Y X)^2)^{-1/2} \text{tr}((X^\top Y \mathcal{K}^2 Y X)^2)^{-1/2}}, \quad (9)$$

where  $\mathcal{K} = XW^\top \text{diag}(a)^2 WX^\top$ .

We assume three properties hold in the finite dimensional case we consider, that will hold asymptotically in the infinite dimensional limit.

**Assumption 9** (Self-averaging). *We assume that computing the average of the NFA quantities across initializations is equal to the quantities themselves in the high-dimensional limit.*

**Assumption 10** (Asymptotic freeness). *We assume that the collections  $\{X, Y\}$  and  $\{W, a\}$  are asymptotically free with respect to the operator  $\mathbb{E}[\text{tr}(\cdot)]$ , where  $\text{tr}[M] = \frac{1}{n} \sum_{i=1}^n M_{ii}$ .*

**Assumption 11** (Commutativity of expectation). *We will also make the approximation that the expectation commutes with ratio and square root.*

$$\mathbb{E}[\rho(A, B)] = \mathbb{E}\left[\frac{\text{tr}(A^\top B)}{\sqrt{\text{tr}(A^\top A)\text{tr}(B^\top B)}}\right] \approx \frac{\mathbb{E}[\text{tr}(A^\top B)]}{\sqrt{\mathbb{E}[\text{tr}(A^\top A)]\mathbb{E}[\text{tr}(B^\top B)]}} \quad (10)$$

We will compute the expected values of the centered NFA under these assumptions. In the remainder of the section we will drop the  $\mathbb{E}[\cdot]$  in the trace for ease of notation.

### E.1. Free probability identities

The following lemmas will be useful: let  $\{\bar{C}_i\}$  and  $\{R_i\}$  be freely independent of each other with respect to  $\text{tr}$ , with  $\text{tr}[\bar{C}_i] = 0$ . Alternating words have the following products:

$$\text{tr}[\bar{C}_1 R_1] = 0 \quad (11)$$

$$\text{tr}[\bar{C}_1 R_1 \bar{C}_2 R_2] = \text{tr}[R_1] \text{tr}[R_2] \text{tr}[\bar{C}_1 \bar{C}_2] \quad (12)$$

$$\text{tr}[\bar{C}_1 R_1 \bar{C}_2 R_2 \bar{C}_3 R_3] = \text{tr}[R_1] \text{tr}[R_2] \text{tr}[R_3] \text{tr}[\bar{C}_1 \bar{C}_2 \bar{C}_3] \quad (13)$$

$$\begin{aligned} \text{tr}[\bar{C}_1 R_1 \bar{C}_2 R_2 \bar{C}_3 R_3 \bar{C}_4 R_4] &= \text{tr}[R_1] \text{tr}[R_2] \text{tr}[R_3] \text{tr}[R_4] \text{tr}[\bar{C}_1 \bar{C}_2 \bar{C}_3 \bar{C}_4] + \\ &\text{tr}[R_1] \text{tr}[R_3] \text{tr}[\bar{R}_2 \bar{R}_4] \text{tr}[\bar{C}_1 \bar{C}_2] \text{tr}[\bar{C}_3 \bar{C}_4] + \text{tr}[R_2] \text{tr}[R_4] \text{tr}[\bar{R}_1 \bar{R}_3] \text{tr}[\bar{C}_2 \bar{C}_3] \text{tr}[\bar{C}_1 \bar{C}_4] \end{aligned} \quad (14)$$

where  $\bar{R}_i \equiv R_i - \text{tr}[R_i]$ .

Applying these identities to the one hidden layer quadratic case, we use the following definitions:

$$R = W^\top \text{diag}(a^2) W, \quad A = (X^\top Y X)^2, \quad B = X^\top X \quad (15)$$

Crucially,  $R$  is freely independent of the set  $\{A, B\}$ . We will also use the notation  $\bar{M}$  to indicated the centered version of  $M$ ,  $\bar{M} = M - \text{tr}[M]$ .

### E.2. Numerator term of NFA

The numerator in Equation (9) is

$$\text{tr}(X^\top Y \mathcal{K} Y X X^\top Y \mathcal{K}^2 Y X) = \text{tr}(ARARBR) \quad (16)$$

Re-writing  $A = \bar{A} + \text{tr}[A]$  and  $B = \bar{B} + \text{tr}[B]$  we have:

$$\text{tr}(X^\top Y \mathcal{K} Y X X^\top Y \mathcal{K}^2 Y X) = \text{tr}((\bar{A} + \text{tr}[A])R(\bar{A} + \text{tr}[A])R(\bar{B} + \text{tr}[B])R) \quad (17)$$

This expands to

$$\begin{aligned} \text{tr}(X^\top Y \mathcal{K} Y X X^\top Y \mathcal{K}^2 Y X) &= \text{tr}(\bar{A}R\bar{A}R\bar{B}R) + 2\text{tr}(A) \text{tr}(\bar{A}R\bar{B}R^2) + \text{tr}(B) \text{tr}(\bar{A}R\bar{A}R^2) \\ &\quad \text{tr}(A)^2 \text{tr}(\bar{B}R^3) + 2\text{tr}(A) \text{tr}(B) \text{tr}(\bar{A}R^3) + \text{tr}(A)^2 \text{tr}(B) \text{tr}(R)^3 \end{aligned} \quad (18)$$

Using the identities we arrive at:

$$\begin{aligned}
 \text{tr}(X^\top Y \mathcal{K} Y X X^\top Y \mathcal{K}^2 Y X) &= \text{tr}[A]^2 \text{tr}[B] \text{tr}(R^3) \\
 &\quad + 2\text{tr}[A] \text{tr}[R^2] \text{tr}[R] \text{tr}(\bar{A}\bar{B}) \\
 &\quad + \text{tr}[B] \text{tr}[R] \text{tr}[R^2] \text{tr}(\bar{A}^2) \\
 &\quad + \text{tr}[R]^3 \text{tr}(\bar{A}^2 \bar{B})
 \end{aligned} \tag{19}$$

### E.3. First denominator term of NFA

The first denominator term in Equation (9) is

$$\text{tr}(X^\top Y \mathcal{K} Y X X^\top Y \mathcal{K} Y X) = \text{tr}(ARAR) \tag{20}$$

This is a classic free probability product:

$$\text{tr}(X^\top Y \mathcal{K} Y X X^\top Y \mathcal{K} Y X) = \text{tr}[A^2] \text{tr}[R]^2 + \text{tr}[A]^2 \text{tr}(R^2) - \text{tr}[A]^2 \text{tr}[R]^2 \tag{21}$$

which can be derived from the lemmas.

### E.4. Second denominator term of NFA

For the second denominator term of Equation (9) we have

$$\text{tr}(X^\top Y \mathcal{K}^2 Y X X^\top Y \mathcal{K}^2 Y X) = \text{tr}(ARBRARBR) \tag{22}$$

Expanding the first  $A$  we have

$$\text{tr}(X^\top Y \mathcal{K}^2 Y X X^\top Y \mathcal{K}^2 Y X) = \text{tr}(\bar{A}RBRARBR) + \text{tr}[A] \text{tr}(R^2 BRARB) \tag{23}$$

Next we expand the first  $B$ :

$$\begin{aligned}
 \text{tr}(X^\top Y \mathcal{K}^2 Y X X^\top Y \mathcal{K}^2 Y X) &= \text{tr}(\bar{A}R\bar{B}RARBR) + \text{tr}[B] \text{tr}(\bar{A}R^2 ARBR) \\
 &\quad + \text{tr}[A] \text{tr}[B] \text{tr}(R^3 ARB) + \text{tr}[A] \text{tr}(R^2 \bar{B}RARB)
 \end{aligned} \tag{24}$$

The next  $A$  gives us

$$\begin{aligned}
 \text{tr}(X^\top Y \mathcal{K}^2 Y X X^\top Y \mathcal{K}^2 Y X) &= \text{tr}(\bar{A}R\bar{B}R\bar{A}RBR) + 2\text{tr}[A] \text{tr}(\bar{A}R\bar{B}R^2 BR) + \text{tr}[B] \text{tr}(\bar{A}R^2 \bar{A}RBR) \\
 &\quad + 2\text{tr}[A] \text{tr}[B] \text{tr}(R^3 \bar{A}RB) + \text{tr}[A]^2 \text{tr}[B] \text{tr}(R^4 B) + \text{tr}[A]^2 \text{tr}(R^2 \bar{B}R^2 B)
 \end{aligned} \tag{25}$$

Expanding the final  $B$  we have

$$\begin{aligned}
 \text{tr}(X^\top Y \mathcal{K}^2 Y X X^\top Y \mathcal{K}^2 Y X) &= \text{tr}(\bar{A}R\bar{B}R\bar{A}R\bar{B}R) + 2\text{tr}[B] \text{tr}(\bar{A}R\bar{B}R\bar{A}R^2) + 2\text{tr}[A] \text{tr}(\bar{A}R\bar{B}R^2 \bar{B}R) \\
 &\quad + 4\text{tr}[A] \text{tr}[B] \text{tr}(R^3 \bar{A}R\bar{B}) + 2\text{tr}[A] \text{tr}[B]^2 \text{tr}(R^4 \bar{A}) + 2\text{tr}[A]^2 \text{tr}[B] \text{tr}(R^4 \bar{B}) \\
 &\quad + \text{tr}[A]^2 \text{tr}[B]^2 \text{tr}[R^4] + \text{tr}[A]^2 \text{tr}[R^2 \bar{B}R^2 \bar{B}] + \text{tr}[B]^2 \text{tr}[R^2 \bar{A}R^2 \bar{A}]
 \end{aligned} \tag{26}$$

Now all terms are in the form of alternating products from the lemma. This means we can factor out the non-zero traces of the other terms. Simplifying we have:

$$\begin{aligned}
 \text{tr}(X^\top Y \mathcal{K}^2 Y X X^\top Y \mathcal{K}^2 Y X) &= \text{tr}[R]^4 \text{tr}((\bar{A}\bar{B})^2) + 2\text{tr}[R]^2 (\text{tr}[R^2] - \text{tr}[R]^2) \text{tr}[\bar{A}\bar{B}]^2 \\
 &\quad + 2\text{tr}[R]^2 \text{tr}[R^2] (\text{tr}[B] \text{tr}(\bar{A}^2 \bar{B}) + \text{tr}[A] \text{tr}(\bar{A}\bar{B}^2)) \\
 &\quad + 4\text{tr}[A] \text{tr}[B] \text{tr}[R^3] \text{tr}[R] \text{tr}(\bar{A}\bar{B}) + \text{tr}[A]^2 \text{tr}[B]^2 \text{tr}[R^4] \\
 &\quad + \text{tr}[A]^2 \text{tr}[\bar{B}^2] \text{tr}[R^2]^2 + \text{tr}[\bar{A}]^2 \text{tr}[B^2] \text{tr}[R^2]^2
 \end{aligned} \tag{27}$$

All terms of the NFA are now in terms of traces of the matrices  $A$ ,  $B$ , and  $R$  and functions on each term separately. The matrices  $A$  and  $B$  are determined by the data, while the moments of the eigenvalues of  $R$  are determined by the initialization distribution of the weights in the neural network, and neither training nor the data.

## F. Balance dataset

The data consists of a mixture of two distributions from which two subsets of the data  $X_1$  and  $X_2$  are sampled from, and is parametrized by a balance parameter  $\gamma \in (0, 1]$  and two variance parameters  $\epsilon_1, \epsilon_2 > 0$ . The subset  $X_1$  which has label  $y_1 = 1$  and constitutes a  $\gamma$  fraction of the entire dataset, is sampled from a multivariate Gaussian distribution with mean 0 and covariance

$$\Sigma = \mathbf{1}\mathbf{1}^\top + \epsilon_1 \cdot I.$$

Then the second subset,  $X_2$ , is constructed such that  $X_2^\top X_2 \approx (X_1^\top X_1)^{-2}$ , and has labels  $y_2 = 0$ . Then, for balance parameter  $\gamma$  sufficiently small, the AGOP second derivative approximately satisfies,

$$\begin{aligned} \mathbb{E} \left[ \dot{W}^\top K \dot{W} \right] &\sim X^\top Y X X^\top X X^\top Y X \\ &= X_1^\top X_1 X^\top X X_1^\top X_1 \\ &\approx X_1^\top X_1 X_2^\top X_2 X_1^\top X_1 \\ &\approx I, \end{aligned}$$

In contrast, the NFM second derivative,  $\mathbb{E} \left[ \dot{W}^\top \dot{W} \right] = (X^\top Y X)^2 = (X_1^\top X_1)^2 \approx \Sigma^2$ , will be significantly far from identity.

Motivated by this derivation, we construct  $X_2$  by the following procedure:

1. Extract singular values  $S_1$  and right singular vectors  $U_1$  from a singular-value decomposition (SVD) of  $X_1^\top X_1$ .
2. Extract the left singular vectors  $V_2$  from a sample  $\tilde{X}_2$  that is sampled from the same distribution as  $X_1$ .
3. Construct  $X_2 = V_2 S_1^{-1} U_1^\top$ .
4. Where  $X = X_1 \oplus X_2$ , Set  $X \leftarrow X + \epsilon_2 Z$ , where  $Z \sim \mathcal{N}(0, I)$ .
5. Set  $y \leftarrow y + 10^{-5} \cdot \mathbf{1}$ .

Note that  $U_1 S_1^{-1} V_2^\top V_2 S_1^{-1} U_1^\top = U_1 S_1^{-2} U_1^\top = (X_1^\top X_1)^{-2}$ , therefore, we should set  $X_2 = V_2 S_1^{-1} U_1^\top$  to get  $X_2^\top X_2 = (X_1^\top X_1)^{-2}$ . Regarding the variance parameters, in practice we set  $\epsilon_1 = 0.5$  and  $\epsilon_2 = 10^{-2}$ .

**Proposition 12** (Expected NFM and AGOP). *For a one hidden layer quadratic network,  $f(x) = a^\top (Wx)^2$ , with  $a \sim \mathcal{N}(0, I)$  and  $W \sim \frac{1}{\sqrt{k}} \cdot \mathcal{N}(0, I)$ ,*

$$\mathbb{E}_{a,W} \left[ \dot{W}^\top \dot{W} \right] = (X^\top Y X)^2,$$

and,

$$\begin{aligned} \mathbb{E}_{a,W} \left[ \dot{W}^\top K \dot{W} \right] &= 3 \cdot \text{tr}(X^\top X) \cdot (X^\top Y X)^2 \\ &\quad + 6 X^\top Y X X^\top X X^\top Y X \end{aligned}$$

*Proof of Proposition 12.*

$$\begin{aligned} \mathbb{E} \left[ \dot{W}^\top \dot{W} \right] &= X^\top Y X \mathbb{E} \left[ W_0^\top \text{diag}(a)^2 W_0 \right] X^\top Y X \\ &= (X^\top Y X)^2. \end{aligned}$$

Further,

$$\mathbb{E} \left[ \dot{W}^\top K \dot{W} \right] = X^\top Y \mathbb{E} \left[ K^2 \right] Y X.$$



We note that,

$$K^2 = W_0^\top \text{diag}(a)^2 W_0 X^\top X W_0^\top \text{diag}(a)^2 W_0 \quad (28)$$

$$= \sum_{s_1, s_2}^k \sum_{\alpha}^n \sum_{p_1, p_2}^d \quad (29)$$

$$a_{s_1}^2 a_{s_2}^2 W_{s_1, p_1} X_{\alpha, p_1} X_{\alpha, p_2} W_{s_2, p_2} X W_{s_1} W_{s_2}^\top X^\top . \quad (30)$$

Therefore, applying Wick's theorem, element  $i, j$  of  $K^2$  satisfies,

$$\begin{aligned} \mathbb{E} [K_{ij}^2] &= \sum_s^k \sum_\alpha^n \sum_{p_1, p_2}^d \mathbb{E} [a_s^4 W_{s, p_1} X_{\alpha, p_1} X_{\alpha, p_2} W_{s, p_2} X_i^\top W_s W_s^\top X_j] \\ &= \sum_s^k \sum_\alpha^n \sum_{p_1, p_2, q_1, q_2}^d \\ &\mathbb{E} [a_s^4 W_{s, p_1} W_{s, p_2} W_{s, q_1} W_{s, q_2} X_{\alpha, p_1} X_{\alpha, p_2} X_{i, q_1} X_{j, q_2}] \\ &= 3 \sum_s^k \sum_\alpha^n \sum_{p_1, p_2, q_1, q_2}^d \\ &\left( \mathbb{E} [W_{s, p_1} W_{s, p_2}] \mathbb{E} [W_{s, q_1} W_{s, q_2}] + \right. \\ &\mathbb{E} [W_{s, p_1} W_{s, q_1}] \mathbb{E} [W_{s, p_2} W_{s, p_2}] + \\ &\left. \mathbb{E} [W_{s, p_1} W_{s, q_2}] \mathbb{E} [W_{s, p_2} W_{s, q_1}] \right) \\ &\cdot X_{\alpha, p_1} X_{\alpha, p_2} X_{i, q_1} X_{j, q_2} \\ &= 3 \sum_\alpha^n \sum_{p_1, p_2, q_1, q_2}^d \\ &\left( \delta_{p_1 p_2} \delta_{q_1 q_2} + \delta_{p_1 q_1} \delta_{p_2 q_2} + \delta_{p_1 q_2} \delta_{p_2 q_1} \right) \\ &\cdot X_{\alpha, p_1} X_{\alpha, p_2} X_{i, q_1} X_{j, q_2} \\ &= 3 \sum_\alpha^n \left( \sum_{p_1, q_1}^d X_{\alpha, p_1} X_{\alpha, p_1} X_{i, q_1} X_{j, q_1} \right. \\ &+ \sum_{p_1, p_2}^d X_{\alpha, p_1} X_{\alpha, p_2} X_{i, p_1} X_{j, p_2} \\ &\left. + \sum_{p_1, p_2}^d X_{\alpha, p_1} X_{\alpha, p_2} X_{i, p_2} X_{j, p_1} \right) \\ &= 3 \cdot \text{tr}(X^\top X) \cdot X_i^\top X_j + 3 \sum_\alpha^n X_\alpha^\top X_i X_\alpha^\top X_j \\ &+ 3 \sum_\alpha^n X_\alpha^\top X_j X_\alpha^\top X_i \\ &= 3 \cdot \text{tr}(X^\top X) \cdot X_i^\top X_j + 3 X_i X^\top X X_j + 3 X_j X^\top X X_i . \end{aligned}$$

Finally, we conclude,

$$\mathbb{E} [K^2] = 3 \left( \text{tr}(X^\top X) X X^\top + 2 X X^\top X X^\top \right) ,$$

giving the second statement of the proposition.  $\square$

## G. Varying the data distribution

We verify that our observations for isotropic Gaussian data hold even when the data covariance has a significant spectral decay. (Figures 9 and 10). We again consider Gaussian data that is mean 0 and where the covariance is constructed from a random eigenbasis. In Figure 9, we substitute the eigenvalue decay as  $\lambda_k \sim \frac{1}{1+k}$ , while in Figure 10, we use  $\lambda_k \sim \frac{1}{1+k^2}$ . We plot the values of the UC-NFA, C-NFA, train loss, and test loss throughout training for the first and second layer of a two hidden layer network with ReLU activations, while additionally varying initialization scale. Similar to Figure 2, we observe that the C-NFA is more robust to the initialization scale than the UC-NFA, and UC-NFA value become high through training, while being small at initialization. We see that the test loss improves for smaller initializations, where the value of the C-NFA and UC-NFA are higher.

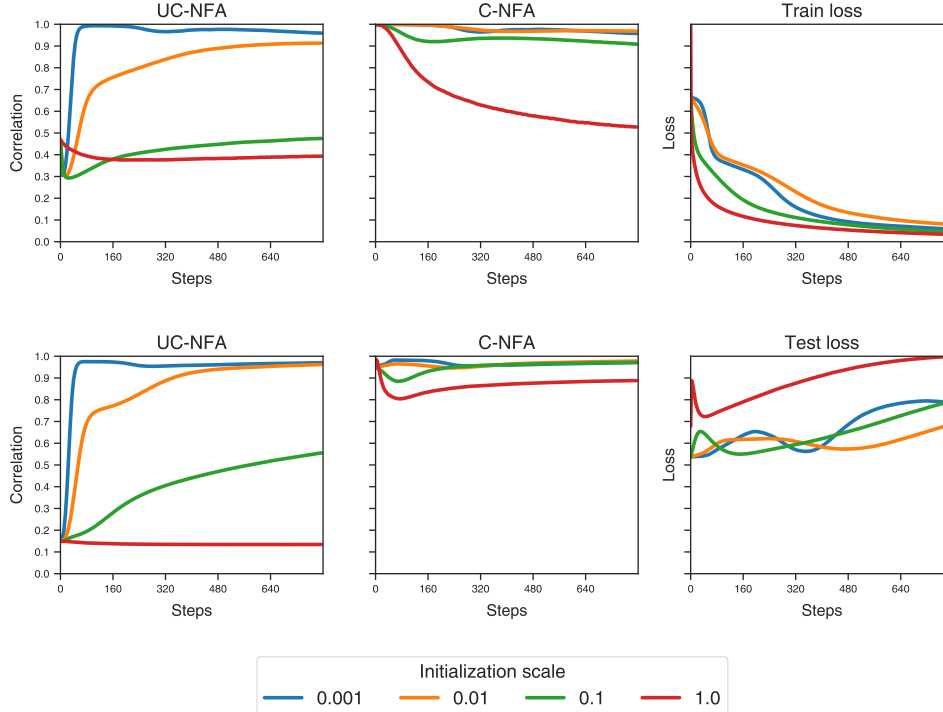


Figure 9. Centered NFA correlations. Data covariance decay rate  $\lambda_k \sim \frac{1}{1+k}$ . Top row is layer 1, bottom row is layer 2. Train (test) losses are scaled by the maximum train (test) loss achieved so that they are between 0 and 1.

## H. Effect of initialization on feature learning

We see that when initialization is small, the C-NFA and UC-NFA are high at the end of training with and without fixing the learning speed (Figure 4). This is reflected by the quality of the features learned by the NFM and the qualitative similarity of the NFM and AGOP at small initialization scale (Figure 11). Further, we notice that as we increase initialization, without fixing speeds, the correspondence between the NFM and decreases and the quality of the NFM features decreases (at a faster rate than the AGOP). Strikingly, when learning speeds are fixed, the quality of the features in the AGOP and NFM becomes invariant to the initialization scale.

## I. Experimental details

We describe the neural network training and architectural hyperparameters in the experiments of this paper. Biases were not used for any networks. Further, in all polynomial tasks, we scaled the label vector to have standard deviation 1.

**Corrupted AGOP** For the experiments in Figure 1, we used  $n = 384$  data points,  $d = 32$ ,  $k = 128$  as the width in all layers, isotropic Gaussian data, initialization scale 0.01 in the first layer and default scale in the second. We used ReLU

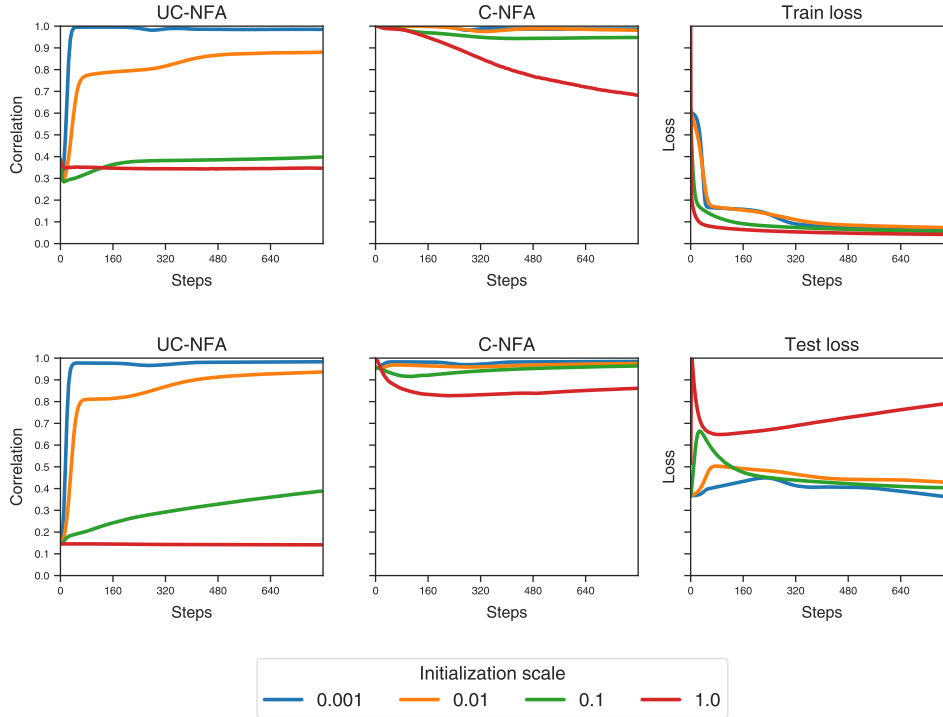


Figure 10. Centered NFA correlations. Data covariance decay rate  $\lambda_k \sim \frac{1}{1+k^2}$ . Top row is layer 1, bottom row is layer 2. Train (test) losses are scaled by the maximum train (test) loss achieved so that they are between 0 and 1.

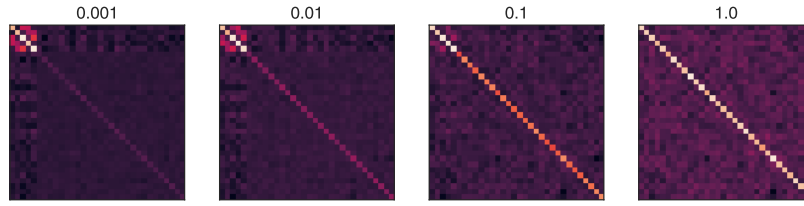
activations and two hidden layers. For the experiments in Figure 2,9,10,6, and 7, we used a two hidden layer network with ReLU activations, learning rate 0.05, 800 steps of gradient descent, and took correlation/covariance measurements every 5 steps.

**Alignment reversing dataset** For the experiments in Figure 3, we used  $k = n = d = 1024$  for the width, dataset size, and input dimension, respectively. Further, the traces of powers of  $F_a$  are averaged over 30 neural net seeds to decouple these calculated values from the individual neural net seeds. The mean value plotted in the first two squares of figure is computed over 10 data seeds.

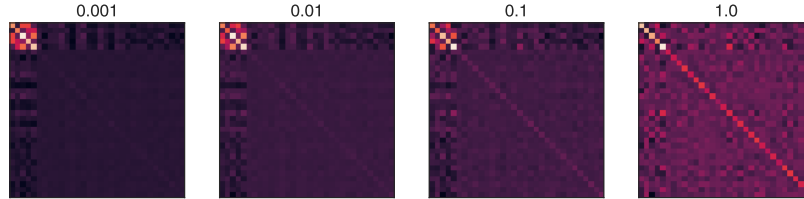
**SLO experiments** For the SLO figures (Figures 5, 11, 4), we use isotropic Gaussian data, 600 steps of gradient descent. The learning rates are chosen based on initialization scale in the first layer. For initialization scales 1, 0.1, 0.01, and 0.001, we used learning rates 0.03, 0.1, 0.2, 0.4, respectively. We again used two hidden layers with ReLU activations. We chose  $n = 256$ ,  $d = 32$ , and  $k = 256$  as the width. We divided the linear readout weights by 0.01 at initialization to promote feature learning, and modified SLO to scale gradients by  $(\epsilon + \|\nabla \mathcal{L}\|)^{-1}$ , rather than just the inverse of the norm of the gradient, for  $\epsilon = 0.1$ . This technique smooths the training dynamics as the parameters approach a loss minimum, allowing the network to interpolate the labels.

**Predictions with depth** For the Deep C-NFA predictions (Figure 8), we used  $n = 128$ ,  $d = 128$ , initialization scale of 1. The low rank task is just the chain monomial of rank  $r = 5$ . The high rank polynomial task is  $y(x) = \sum_{i=1}^d (Qx)_i^2$ , where  $Q \in \mathbb{R}^{d \times d}$  is a matrix with standard normal entries.

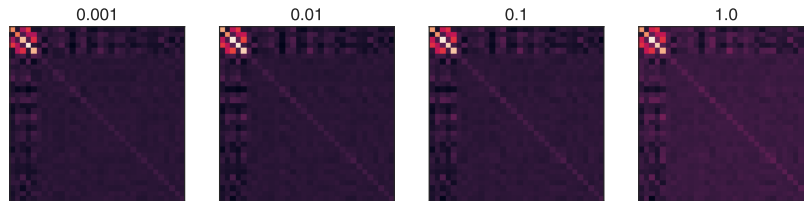
**Real datasets** For the experiments on the SVHN dataset, we train a four hidden layer neural network with ReLU activations, initialization scale 1.0 in all layers and width 256. For SVHN, we subset the dataset to 4000 points. We train for 3000 epochs with learning rate 0.2 for standard training, and 0.3 for SLO, and take NFA measurements every 50 epochs. For SLO, we set  $C_0 = 2.5$ ,  $C_1 = C_2 = 0.4$ , and relaxation parameter  $\epsilon = 0.2$ . We pre-process the dataset so that each pixel is mean 0 and standard deviation 1. For the experiments on CelebA, we train a two hidden layer network on a balanced subset



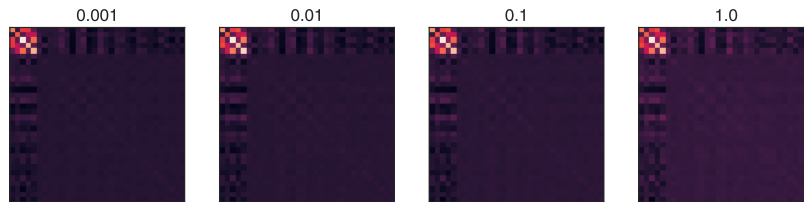
(a) NFM, speeds not fixed.



(b) AGOP, speeds not fixed.



(c) NFM, speeds fixed.



(d) AGOP, speeds fixed.

Figure 11. The NFM at the end of training as a function of initialization scale in the first layer weights, with and without fixing learning speeds. The task again is the chain monomial with rank  $r = 5$ . The title of each plot is the initialization scale of the first layer  $s_0$ .

of 7500 points with Adam with learning rate 0.0001 and no weight decay. We use initialization scale 0.02 in the first layer, and width 128. We train for 500 epochs. We pre-process the dataset by scaling the pixel values to be between 0 and 1.

## J. Additional SLO experiments

We demonstrate the SLO can be applied adaptively to increase the strength of the UC-NFA in all layers of a deep network on the chain monomial task of rank  $r = 3$ . We train a three hidden layer MLP with ReLU activations and an initialization scale of 0.1 by SLO, and find that all layers finish at the same high UC-NFA (Figure 12). Further, this final UC-NFA value is higher than the highest UC-NFA achieved by any layer with standard training. The generalization loss is also lower with SLO on this example, corresponding to better feature learning (through the UC-NFA).

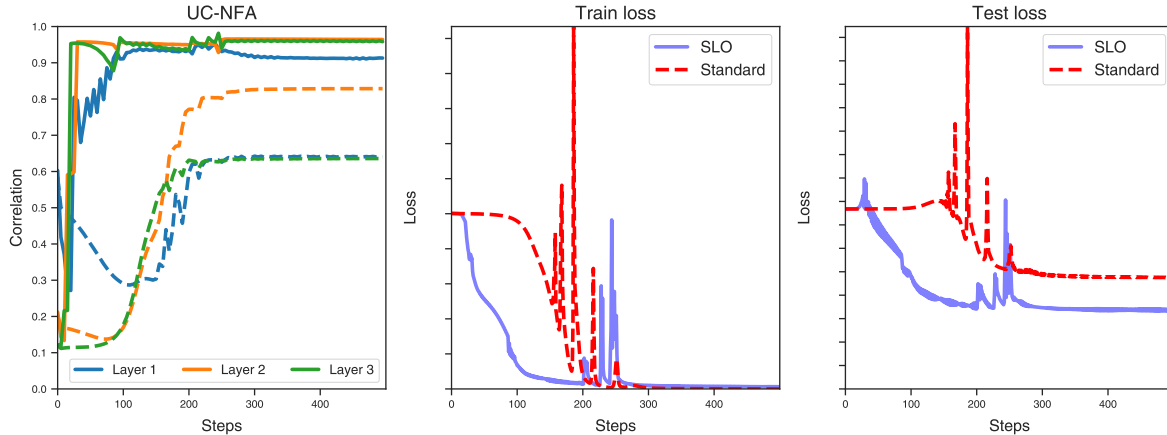


Figure 12. Training with SLO where the learning speeds are chosen adaptively based on the UC-NFA values of all layers. The dashed lines correspond to training with standard GD.

At every time step we choose  $C_i = s$  for the layer  $i$  with the smallest UC-NFA correlation value, while setting  $C_j = s^{-1}$  for all other layers, with  $s = 20$ . We again modify SLO by dividing the gradients by  $\epsilon \|\nabla \mathcal{L}\|$  for  $\epsilon = 0.01$ . The learning rate is set to 0.05 in SLO and 0.25 for the standard training (gradient descent), and the networks are trained for 500 epochs. We sample  $n = 256$  points with  $d = 32$ , and use width  $k = 256$ .

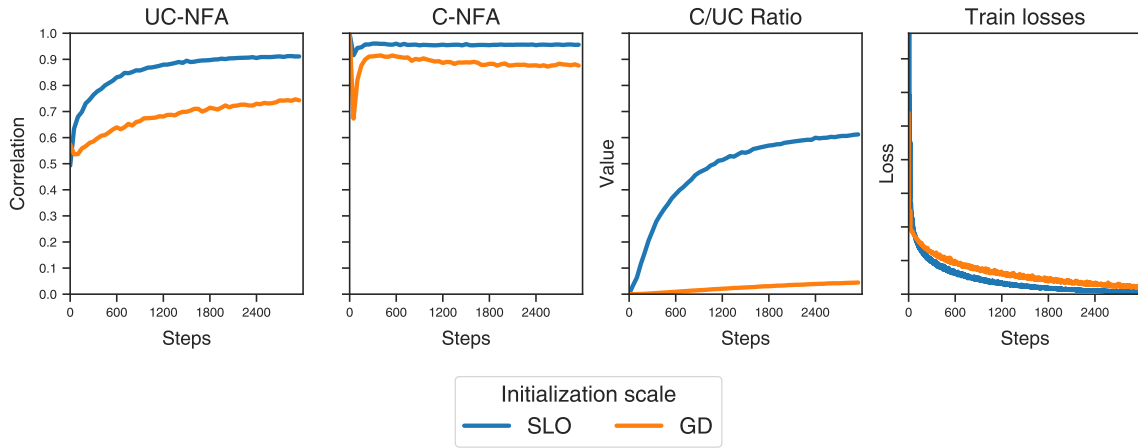


## K. Experiments on real datasets

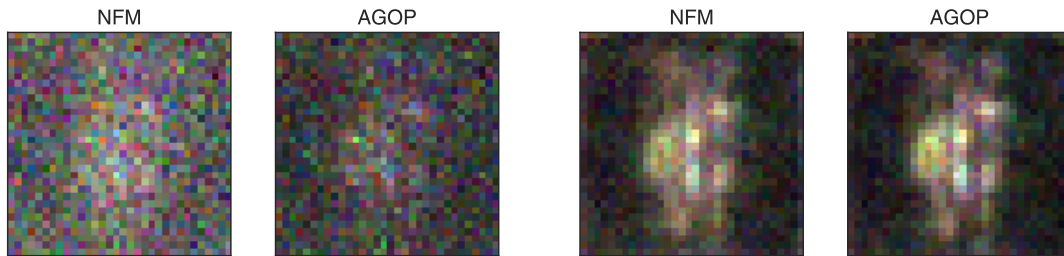
We replicate Figures 1, 4, and 5 on celebrity faces (CelebA) and Street View House Numbers (SVHN). We begin by showing that one can disrupt the NFA correspondence by replacing the PTK feature covariance with a random matrix of the same spectral decay. For this example, we measure the Pearson correlation, which subtracts the mean of the image. I.e.  $\bar{\rho}(A, B) \equiv \rho(A - m(A), B - m(B))$ , where  $m(A), m(B)$  are the average of the elements of  $A$  and  $B$ .



Figure 13. Various feature learning measures for the CelebA binary subtask of predicting glasses. The diagonals of the NFM ( $W^T W$ ) (first plot) and AGOP ( $W^T K W$ ) (second plot) of a fully-connected network are similar to each other. Replacing  $K$  with a symmetric matrix  $Q$  with the same spectrum but independent eigenvectors obscures the low rank structure (third plot), and reduces the Pearson correlation of the diagonal from  $\bar{\rho}(\text{diag}(F), \text{diag}(\bar{G})) = 0.91$  to  $\bar{\rho}(\text{diag}(F), \text{diag}(W^T Q W)) = 0.04$ .



(a) Feature learning measurements.



(b) Standard Training

(c) SLO

Figure 14. We demonstrate on the SVHN dataset, with a 4 hidden layer neural network with large initialization scale, how SLO can improve the strength of the UC-NFA, the C-NFA, the ratio of the unnormalized C-NFA to UC-NFA (plot (a)) and the feature quality (plots (b) and (c)). In plots (b) and (c), we visualize the diagonal of the NFM and AGOP for the first layer of the trained network, where SLO was applied with  $C_0 = 2.5$ ,  $C_1 = C_2 = 0.4$ .